# <arttitle> superconductivity in doped cubic silicon

<aug> E. Bustarret[1], C. Marcenat[2], P. Achatz[1,2], J. Kačmarčik[1,3], F. Lévy[2], A. Huxley[2], L. Ortéga[4], E. Bourgeois[5], X. Blase[5], D. Débarre[6], J. Boulmer[6]

*<aff> [1]Laboratoire d'Etudes des Propriétés Electroniques des Solides, CNRS, BP166 38042 Grenoble Cedex 9, France. [2]DRFMC-SPSMS, CEA Grenoble, 17 rue des Martyrs, 38054 Grenoble Cedex 9, France. [3]Institute of Experimental Physics, Slovak Academy of Sciences, SK- 04001 Košice, Slovakia. [4]Laboratoire de Cristallographie, CNRS, BP166 38042 Grenoble Cedex 9, France. [5]Laboratoire de Physique de la Matière Condensée et Nanostructures, Université Lyon I ; CNRS, Domaine scientifique de la Doua, 69622 Villeurbanne Cedex ; France. [6]Institut d'Electronique Fondamentale, Université Paris Sud and CNRS, Bât. 220, 91405 Orsay, France.*

*<aff> "footnote" The two first authors E.Bu. and C.M. contributed equally to this work*

**<abs> Today's micro-electronics are largely based on the ability to locally modify the electronic properties of silicon. Although the local resistivity of semiconducting silicon in its standard crystalline form can be changed by many orders of magnitude by doping with elements, known as electron acceptors and donors, superconductivity has so far never been achieved and hybrid devices combining silicon's semiconducting properties and superconductivity have therefore remained largely underdeveloped. Here we report that superconductivity can be induced when boron is locally introduced into silicon at concentrations above its equilibrium solubility. For high-enough boron doping (typically 100 ppm) silicon becomes metallic down to low temperature. Our new finding is that at a higher boron concentration of several percent, achieved by gas immersion laser doping, silicon becomes superconducting. Our electrical resistivity and magnetic susceptibility measurements show that boron-doped silicon (B:Si) made in this way**

**is a superconductor below a transition temperature $T_c \approx 0.35$ K, with a critical field ≈ 0.4 Tesla. Ab initio calculations, corroborated by Raman measurements, strongly suggest that doping is substitutional. The calculated electron-phonon coupling strength is found to be consistent with a conventional phonon-mediated coupling mechanism. Since high quality interfaces between the new superconducting silicon and other variously doped or oxidized silicon regions can be made, our findings will facilitate the fabrication of new silicon-based superconducting nanostructures and mesoscopic devices.**

<p> Semiconductors, such as GeTe, PbTe and $SrTiO_3$, have been shown in the past to become superconducting at low temperature upon carrier doping[1-3]. In contrast, superconductivity has been sought for in silicon for sixty years[4] but observed only in its β-Sn and hexagonal (sh) metallic phases obtained under extreme pressures[5-7] of the order of 10 GPa. This is surprising given that theoretical calculations have consistently predicted doped germanium[8] and silicon[9,10] to be superconducting in their fcc (ambient pressure) diamond structure and that conventional superconductivity has been found in materials that contain light group IV elements, such as silicon clathrates[9,11] and boron-doped diamond[12-14].

Here we report structural, electrical and magnetic experiments performed at room pressure on a set of B-doped silicon thin layers where boron was incorporated into cubic silicon well above its equilibrium solubility (1.2 at.% or 6 $10^{20}$ $cm^{-3}$). As depicted in Figure 1, this was achieved by Gas Immersion Laser Doping (GILD) where the precursor gas ($BCl_3$) is chemisorbed on a (001)-oriented silicon wafer prior to each UV laser pulse[15-17]. During each melting/solidification cycle, boron diffuses into molten silicon, and is incorporated at substitutional sites of the crystal as the liquid/solid

interface moves back to the surface of the epilayer[15]. The in-plane lattice matching to the substrate and the local incorporation of boron atoms of lower covalent radius[18] results in the formation of biaxially strained pseudomorphic layers[15,17] with thicknesses ranging from 10 to 120 nm.

High Resolution XRD analysis of three samples was performed around the (004) Bragg reflection. As shown in Figure 1, we observed one or two broad diffraction peaks well separated from the narrow line from the substrate. This indicates a non-uniform distribution of the strain perpendicular to the surface and thus of the boron content, but confirms the epitaxial single crystal character of the films. The two broad maxima detected in sample #1 at 35.56 and 36.02° correspond to a contraction of the lattice parameter, a, along (001) of da/a = -2.5 and -3.7 % respectively. Assuming that the Si:B alloy retains the elastic properties of bulk silicon, this yields an in-plane tensile stress ("negative" pressure) of 2.6 and 3.9 GPa, and isotropic lattice parameter variations of -1.4 and -2.1 %. From Vegard's law and previous calibrations[15,17,18], this corresponds to substitutional boron concentrations of 5.7 and 8.4 at.% (i.e. 2.8 $10^{21}$ and 4.2 $10^{21}$ B/$cm^3$). Hall measurements performed at room-temperature on the same sample (#1) give a free-hole density of the order of 5±2 $10^{21}$ $cm^{-3}$, which is comparable to the higher Boron concentration deduced above. The XRD results shown in Fig. 1 indicate that sample #2 has a slightly lower B concentration, while #3 has a much lower concentration than sample #1.

We now discuss the electrical characterisation of the samples. The~~ir~~ room-temperature sheet resistances of sample #1, 2 and 3 are 35, 17 and 8 Ω/□ respectively, while their resistivities are of the order of 100 μΩcm with temperature dependences from 300 K to 0.35 K typical of disordered metals (see fig. 2). The inset of figure 2 shows measurements made to lower temperature with a dilution refrigerator. Two of the samples (#1 and #2) undergo superconducting transitions to zero resistance, respectively

at 150 and 45 mK, whereas sample #3 shows only a partial transition. It should be noted that elemental boron becomes superconducting[19] only under a very high pressure of the order of 160 GPa and therefore cannot account for this superconductivity.

The temperature dependence below 0.5 K of the direct-current electrical resistance, R, and of the real part of the ac-magnetic susceptibility, $\chi$', for sample #1 is plotted in Fig. 3a. A sharp drop of the resistance is observed with an onset around 0.4 K. An immeasurably small R value is observed below 150mK. Similarly as the temperature decreases there is an onset of diamagnetism below 0.34 K, but full magnetic screening is not achieved until 150mK. These measurements unambiguously demonstrate the occurrence of superconductivity in sample #1. The foot of the resistive and diamagnetic transitions and the width of the magnetic response are typical of an inhomogeneous superconductor[20] : this inhomogeneity is expected given the non-uniform boron distribution detected by XRD. In order to define the phase diagram in the magnetic field-temperature (H-T) plane, we performed electrical measurements varying the temperature at different magnetic fields, ~~H,~~ and varying H at different temperatures (see the insets in Fig.2b) with the field applied perpendicular to the plane of the film. The transitions remain sharp and no hysteresis or supercooling was seen, which is consistent with the transition to superconductivity under field being of second order. This observation, and the relatively high value of the critical field, 0.4 Tesla (see fig. 3b), which exceeds that of Lead (800 Gauss), the strongest known type I superconductor, suggests that boron-doped silicon is a type II superconductor. The critical temperature $T_{c2}$ and the critical magnetic field $H_{c2}$ where the resistance is 10% of its normal state value are plotted in Fig. 3b (the 10% criterion corresponds to the onset of diamagnetism in zero field ). To indicate the width of the transition, the positions of maxima of the slope of the resistance versus temperature (dR/dT) in the T-sweeps and maxima of dR/dH in the H-sweeps are also shown (open symbols in Fig. 3b). The critical field versus temperature curve in Fig. 3b has a marked curvature compared with the standard Bardeen-Cooper-Schriefer (BCS) dependence[21]. This feature could be explained by paramagnetic limitation if the carriers are assigned a gyromagnetic factor, g, 40% larger[22] than the standard value of 2. Alternatively, the observed dependence might be a consequence of the film's inhomogeneity : it could arise if the dimensions of the

superconducting regions are restricted parallel to the film surface, or be due to percolation or localisation phenomena[23,24]. The Landau-Ginzburg superconducting coherence length is estimated in the orbital limit to be 13 nm from the experimentally measured slope of $H_{c2}$ against temperature at $T_c$ while a larger estimate of approximately 20 nm is found based on the values of $T_c$ and $H_{c2}(0)$ (at zero temperature) within the standard BCS theory. These values are not much smaller than the estimated thickness of the film (35 ±5 nm), which can also act to limit the extent of the coherence length[25].

In order to provide some insight into the microscopic pairing mechanism, we performed an ab initio study of the electronic, vibrational and electron-phonon coupling properties of boron-doped silicon. We adopted a supercell approach with one B atom substituted for every 16 silicon atoms arranged in a fcc cell, yielding a 6.25 at.% concentration, close to the values estimated for the superconducting samples (see Methods). Structural relaxation led to an isotropic contraction of 1.9 % of the lattice parameter compared to the pure Silicon, related to the reduced Si-B bond length (2.1 Å in our calculations), and within the range of values deduced experimentally by XRD.

Close to the Fermi level that is located 0.5 eV below the top of the valence bands, the calculated band structure resembles that of undoped silicon, confirming the degenerate nature of Si:B at such a high doping level. The phonon density of states (*p*DOS) is represented in Fig.4. As compared to undoped silicon, we found a ~ 42 $cm^{-1}$ softening of the zone-center optical modes. The softening is caused by hole injection which more than compensates the effect of lattice contraction. As illustrated in Fig. 4, the calculated softening agrees well with the broadened Raman peaks observed in samples #1, #2 and #3 at 464, 480 and 485 $cm^{-1}$ respectively, and can be compared with a peak position of 520 $cm^{-1}$ in pure Si. Experimentally, the shift to lower frequency and the broadening are more pronounced for sample #1 which has the highest $T_c$. The appearance of an additional Raman-active Si-B stretching mode 100 $cm^{-1}$ above the zone-centre optical

modes, seen experimentally, is found in the calculation to correspond to a Si-B stretching mode at around 590-600 $cm^{-1}$.This observation further confirms the substitutional incorporation of boron.

To estimate the superconducting transition temperature, we calculated the electron-phonon coupling function (Eliashberg function), which measures the coupling strength as a function of the phonon energy (Fig. 4). As for boron-doped diamond[10,26,27], most of the coupling originates from the optical modes. Averaging over the Brillouin zone and phonon bands, we find a coupling constant $\lambda$ of 0.28. This is in good agreement with $\lambda$=0.30 for 5%-doping within the virtual crystal approximation[10]. The peaked structure of the Eliashberg function around $\omega_0$= 470 $cm^{-1}$ suggests the use of the following modified McMillan formula appropriate for a $\delta$-shaped spectrum : $T_c = \hbar\omega_0 \exp[-(1+\lambda)/(1-\mu^*(1+\lambda)]$, where $\mu^*$ accounts for the screened Coulomb repulsion. We find that for $\mu^*$ in the range 0.08-0.12 (a value of $\mu^* = 0.1$ was adopted by Boeri et al[10]), $T_c$ is predicted to vary in the range 0.34 – 0.03 K. This suggests that a standard BCS mechanism can account for the observed superconducting transition. Theory[10] as well as experimental results obtained on superconducting B-doped diamond[28] lead us to expect that a higher superconducting transition temperature might be achieved if more boron could be incorporated into the silicon. This is an exciting possibility as it would considerably facilitate the development of Si:B nanostructures and mesoscopic devices exploiting superconductivity.

## <meth1ttl> Methods

### Sample preparation and characterization

Laser-induced doping was performed with a 308 nm wavelength laser over ten separate 6 $mm^2$ areas of the same wafer in a special GILD configuration. The precursor gas ($BCl_3$) was injected and chemisorbed on a {001}-oriented silicon wafer surface prior to each of the 200 laser shots of 25 ns duration. In situ monitoring of the transient reflectivity at 675 nm, as well as previous calibrations by Secondary Ion Mass Spectroscopy[17], enabled us to adjust the power and duration of the pulses in order to ensure maximum doping over the whole thickness of the melt. Estimated thicknesses for samples #1, 2 and 3 were 30±5 nm, 30±5 nm and 110±10 nm respectively. Micro-Raman backscattering spectra excited by a cw HeCd laser (3 mW at 325 nm) were collected at room temperature in air under a x40 microscope objective. We used a HR800-UV Jobin-Yvon-Horiba spectrophotometer equipped with an edge filter and a liquid $N_2$-cooled 256x2048 pixel CCD detector. The spectral resolution was better than 2 $cm^{-1}$. High resolution X-ray diffraction measurements were performed with a commercial Philips Materials research diffractometer at the Cu $K_{\alpha 1}$ wavelength of 0.15406 nm selected with a (220) Ge 4-reflection Bartels-type monochromator. Rocking curves were obtained by measuring the diffracted intensity as a function of the rotation, $\theta$, of the sample. Data were collected around the (004) silicon Bragg reflection with an angular resolution better than 3 $10^{-3}$ degree. The absence of polycrystalline phases was checked by additional diffraction measurements at grazing incidence.

**Electrical and magnetic measurements**

Electrical resistivity measurements were performed from room temperature down to 0.35 K using a Quantum Design Physical Properties Measurements System and were extended down to 40 mK in dilution refrigerators using standard lock-in techniques. Gold wires were attached onto the samples in a 4-terminal configuration either directly with silver epoxy or on evaporated Au:Ti contacts for a better definition of geometrical factors. To avoid artefacts, various careful checks were made such as the comparison of

a.c. and d.c. electrical measurements as well as current-voltage I(V) characteristics. The normalised resistance values displayed in Fig. 3a result from d.c. measurements with I=100 nA.

Measurements of a.c. magnetic susceptibility were obtained by recording the change in the mutual inductance of a small coil at 9 kHz with a Stanford Research 836 lock-in amplifier. The coil response was calibrated by measuring a thin film of Niobium with similar size and shape. All magnetic measurements were performed with the magnetic field perpendicular to the film plane.

**Ab initio calculations**

Our calculations were based on an ultrasoft pseudopotential planewave implementation of density functional theory with a generalized-gradient description of the exchange-correlation functional. They were performed with the Plane Wave Self-Consistent Field package (www.pwscf.org). The Perdew Burke Ernzerhof functional was used, together with a 25 Ryd and a 200 Ryd cut-off for the eigenstates and charge density respectively. Electronic and phonon momentum were sampled with a 5x5x5 and 4x4x4 Monkhorst-Pack grid respectively. The electronic sampling was increased to 10x10x10 for evaluating $\lambda$. Within the present approach, the zone center optical modes for pure cubic silicon are found at 502 $cm^{-1}$ , compared to the experimental value of 520 $cm^{-1}$. For the sake of comparison with experiment, the theoretical frequencies have been rescaled by 520/502=1.036 in figure 4.

<corr> Correspondence should be addressed to E.Bu. (etienne.bustarret@grenoble.cnrs.fr) and to C.M. (christophe.marcenat@cea.fr).

<bibcit> 1. Hein, R.A., Gibson, J.W., Mazelsky, R., Miller, R.C. & Hulm, J.K., Superconductivity in Germanium Telluride, *Phys. Rev. Lett.* **12**, 320-2 (1964).

2. Schooley, J.F.et al., Dependence of the Superconducting Transition Temperature on Carrier Concentration in Semiconducting $SrTiO_3$, *Phys. Rev. Lett.* **14**, 305-7 (1965).

3. Lasbley, A., Granger, R. & Rolland, S., High temperature superconducting behaviour in PbTe-Pb system, *Sol. State Comm*. **13**, 1045-8 (1973).

4. Alekseyevsky, N. & Migunov, L., Investigation of metals at temperatures below 1°K. *J. Phys. (USSR)* **11**, 95 (1947).

5. Buckel, W. & Wittig, J., Supraleitung von Germanium und Silizium unter hohem Druck. *Phys. Lett.* **17,** 187-8 (1965).

6. Stepanov, G.N., Valyanskaya, T.V. & Yakovlev, E.N., Superconductivity of metallic silicon below the pressure of transition to metallic modification. *Sov. Phys. Solid State* **22**, 292-3 (1980).

7. Chang, K.J. et al., Superconductivity in High-Pressure Metallic Phases of Si. *Phys. Rev. Lett.* **54**, 2375-8 (1985).

8. Cohen, M. L., Superconductivity in Many-Valley Semiconductors and in Semimetals. *Phys. Rev.* **134**, A511-21 (1964).

9. Connétable, D. et al., Superconductivity in Doped $sp^3$ Semiconductors : The Case of the Clathrates. *Phys. Rev. Lett.* **91**, 247001 (2003).

10. Boeri, L., Kortus, J. & Andersen, O.K., Three-Dimensional $MgB_2$-Type Superconductivity in Hole-Doped Diamond. *Phys. Rev. Lett*. **93**, 237002 (2004).

11. Kawaji, H., Horie, H., Yamanaka, S. & Ishikawa, M., Superconductivity in the silicon clathrate compound $(Na,Ba)_xSi_{46}$. *Phys. Rev. Lett.* **74**, 1427–9 (1995).

12. Ekimov, E.A. et al., Superconductivity in diamond. *Nature* **428**, 542-5 (2004).

13. Yokoya, T. et al., Origin of the metallic properties of heavily boron-doped superconducting diamond. *Nature* **438**, 647-50 (2005).

14. Sacépé, B. et al., Tunneling Spectroscopy and Vortex Imaging in Boron-Doped Diamond. *Phys. Rev. Lett.* **96**, 097006 (2006).

15. Kerrien, G. et al., Ultra-shallow, super-doped and box-like junctions realized by laser-induced doping, *Appl. Surf. Sci.* **186**, 45-51 (2002).

16. Kerrien, G. et al., Gas immersion laser doping (GILD) for ultra-shallow junction formation. *Thin Sol. Films* **453-454**, 106-9 (2004).

17. Kerrien, G. et al., Optical characterization of laser-processed ultrashallow junctions. *Appl. Surf. Sci.* **208-209**, 277-84 (2003).

18. Vailionis, A., Glass, G., Desjardins, P., Cahill, D.G. & Greene, J.E., Electrically Active and Inactive B Lattice Sites in Ultrahighly B Doped Si(001): An X-Ray Near-Edge Absorption Fine-Structure and High-Resolution Diffraction Study. *Phys. Rev. Lett.* **82**, 4464-7 (1999).

19. Eremets, M.I., Struzhkin, V.V., Mao Ho-kwang & Hemley, R.J., Superconductivity in Boron. *Science* **293**, 272-4 (2001).

20. Tinkham, M, Introduction to inhomogeneous superconductors, in "Inhomogeneous Superconductors-1979", edited by Gubser, D.U., Francavilla, T.L., Laibowitz, J.R. & Wolf, S.A., *AIP Conf. Proc.* **58**, 1-12 (1980).

21. Werthamer, N.R., Helfand, E. & Hohenberg, P.C., Temperature and Purity Dependence of the Superconducting Critical Field $H_{c2}$, III. Electron Spin and Spin-Orbit Effects. *Phys. Rev.* **147**, 295-302 (1966).

22. Ting, C.S., Lee, T.K. & Quinn, J.J., Effective Mass and g Factor of Interacting Electrons in the Surface Inversion Layer of Silicon. *Phys. Rev. Lett.* **34**, 870-4 (1975).

23. Kent, A.D., Kapitulnik, A. and Geballe, T.H., $H_{c2}$ spectroscopy of Geometrical Effects in La-S Films. *Phys. Rev.* **B36**, 8827-30 (1987).

24. Quateman, J.H., $T_c$ suppression and critical fields in thin superconducting Nb films. *Phys. Rev.* **B34**, 1948-51 (1986).

25. Guyon, E., Meunier, F. & Thomson, R.S., Thickness Dependence of $\kappa_2$ and Related Problems for Superconducting Alloy Films in Strong Fields. *Phys. Rev.* **156**, 452-69 (1967).

26. Blase, X., Adessi, Ch. & Connétable, D., Role of the Dopant in the Superconductivity of Diamond. *Phys. Rev. Lett.* **93**, 237004 (2004).

27. Lee, K.-W. & Pickett, W.E., Superconductivity in Boron-Doped Diamond. *Phys. Rev. Lett.* **93**, 237003 (2004).

28. Bustarret, E. et al., Dependence of the Superconducting Transition Temperature on the Doping Level in Single-Crystalline Diamond Films. *Phys. Rev. Lett.* **93**, 237005 (2004).

<ack> The authors gratefully acknowledge Drs J. Marcus, M. Sanquer and X. Jehl for the access to their cryostats, as well as Dr J. Pernot for stimulating discussions. The samples were prepared by D.D. and J.B. and the calculations performed by E.Bo. and X.B. at the CNRS national supercomputing centre (IDRIS). All other authors contributed to the physical characterisation of the samples. A.H.'s present address is : School of Physics, University of Edinburgh, Edinburgh EH9 3JZ, UK. Partial funding by french ANR-05-BLAN-program is acknowledged.

<LEGEND> Figure 1 : High resolution XRD measurements around the (004) Bragg reflection of three Si:B superconducting samples labelled #1, #2 and #3. Inset :schematics of the 3 initial stages of Gas Immersion Laser Doping (GILD).

The rocking curves are vertically offset for clarity. Lineshape analysis of the diffraction peaks led to the following Bragg angle positions : 34.565° (Si substrate) ; 35.56 and 36.02° (sample #1) , 35.23 and 35.97° (#2) ; 35.30 and 35.47° (#3). The stronger intensity measured on sample #3 results from its larger thickness (100-120 nm). The three initial steps of GILD, which are then repeated about 200 times to produce the Si:B samples studied, are : adsorption of $BCl_3$ on the silicon wafer surface (left) ; local surface melting of silicon induced by the laser shot (center) ; formation of the Si:B epilayer upon cooling (right).

Figure 2 : Temperature dependence of the a.c. resistivity $\rho$ showing the metallic behaviour of crystalline silicon doped with boron in the at.% range (sample #1). Inset : T-dependence of the a.c. resistivity at low temperatures for samples #1, 2 and 3, normalised to their normal state resistivity $\rho_n$ at 2K.

Figure 3 : .Superconducting transition and magnetic phase diagram of B-doped Si (sample #1). **a.** Temperature dependence of the d.c. electrical resistance R (normalised to its normal state value $R_n$) and of the real part of the a.c.-susceptibility. **b.** Temperature dependence of the upper critical field $H_{c2}$ : squares : $H_{c2}$ measured by field sweeps at 50, 150, 200, 250, 300 and 350 mK (see lower inset) ; circles : $T_{c2}$ measured by temperature sweeps at 0.1, 0.2, 0.3, 0.4 and 0.5 Tesla (see upper inset). ; open symbols : location of dR/dT and dR/dH maxima ; full line : classical theory[17].

Figure 4 : Calculated and experimental vibrational spectral density of B:Si. Phonon density of states (thick grey line) and Eliashberg function (broken line) as calculated ab initio for a $B:Si_{15}$ supercell, compared to experimental UV-Raman spectra of samples #1, 2 and 3 in the 350-650 $cm^{-1}$ range. For the sake of comparison with experiment, the theoretical frequencies have been rescaled

by 520/502=1.036. Please note that at the present excitation energy (3.82 eV), the absorption length in Si:B is so short that no signal from the substrate could be detected in all the samples.

Fig. 1

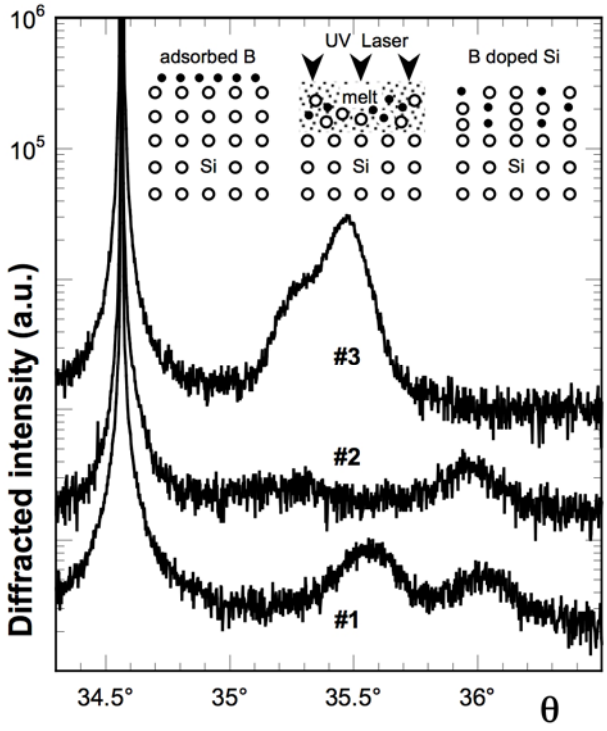
$10^6$
$10^5$
Diffracted intensity (a.u.)
adsorbed B
UV Laser
B doped Si
melt
Si
Si
Si
#3
#2
#1
34.5°
35°
35.5°
36°
θ

Fig. 2

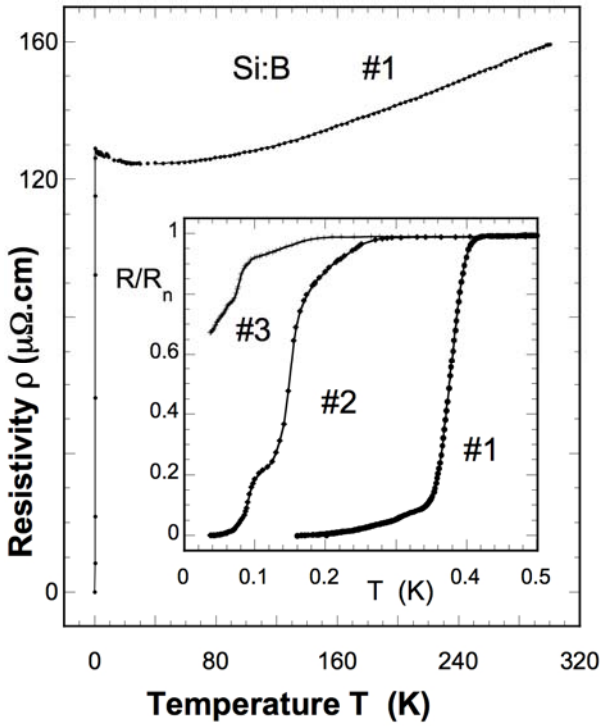

Fig. 3

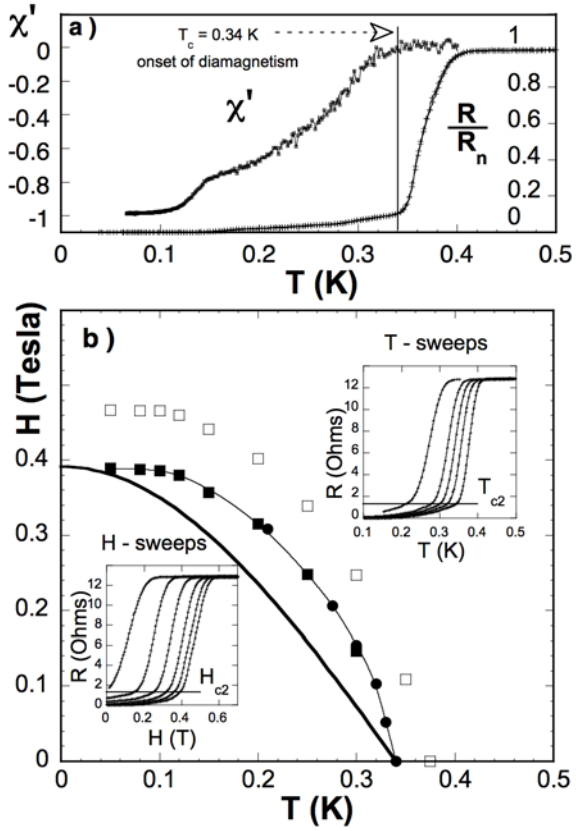
a )
T_c = 0.34 K
onset of diamagnetism
χ'
R/R_n
T (K)
b )
T - sweeps
R (Ohms)
T_c2
T (K)
H - sweeps
H_c2
H (T)
H (Tesla)
T (K)

Fig. 4

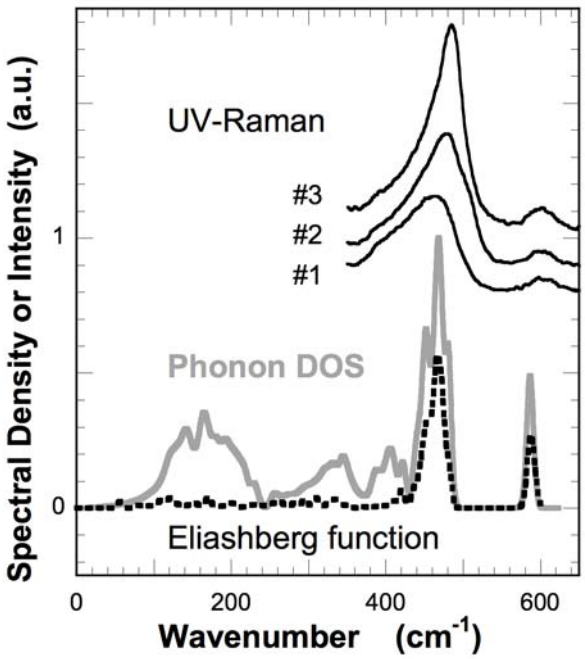
Spectral Density or Intensity (a.u.)
UV-Raman
#3
#2
#1
Phonon DOS
Eliashberg function
1
0
0
200
400
600
Wavenumber (cm-1)